SUPPORTING INFORMATION

Targeting G-Quadruplex structures with Zn(II) terpyridine derivatives: a SAR study

Natalia Busto[a*], M. Carmen Carrión[b], Sonia Montanaro[c], Borja Diaz de Greñu,[b] Tarita Biver[c, d], Felix A. Jalón[b*], Blanca R. Manzano[b*] and Begoña García[a*].

[a]Chemistry Department, University of Burgos, Pza. Misael Bañuelos s/n, 09001 Burgos, Spain (nataliabyv@msn.com; begar@ubu.es)

[b] Departamento de Química Inorgánica, Orgánica y Bioquímica, Facultad de Químicas (IRICA), Universidad de Castilla La Mancha, Avenida Camilo J. Cela 10, 13071 Ciudad Real, Spain (blanca.manzano@uclm.es; felix.jalon@uclm.es)

[c] Department of Chemistry and Industrial Chemistry, University of Pisa, Via Moruzzi, 13, 56124 Pisa, Italy

[d] Department of Pharmacy, University of Pisa, Via Bonanno Pisano 6, 56126 Pisa, Italy

Table of Contents

Synthesis and characterization of ligands L1-L3

L1 and **L2**. These ligands were prepared following an improved method as reported in the literature.[1, 2,3] The reaction of 2-acetylpyridine (40 mmol) with 4-(1H-imidazol-1-yl)benzaldehyde or 4-pyridincarboxaldehyde (20 mmol) was carried out in ethanol (100 mL) at 40 °C overnight in the presence of NaOH (40 mmol) and concentrated aq NH_3 (50 mmol). The resulting precipitate was filtrated and washed with water (4 × 10 mL) and EtOH (2 × 5 mL) giving pale yellow solids. These solids were recrystallized in dichloromethane (DCM)/EtOH to obtain a white powder that was filtrated and dried under vacuum (10.5 mmol). The NMR data are included as those reported were in a different solvent. ^{1}H NMR: **L1** δ(CD_3OD, TMS). 8.78 (s, $H^{3',5'}$ tpy, 2H), 8.75 (d, $H^{a\ or\ b}$ py, J_{HH} = 4.7, 2H), 8.72 (d, $H^{6,6''}$ tpy, J_{HH} = 5.6, 2H), 8.69 (d, $H^{3,3''}$ tpy, J_{HH} = 8.0, 2H), 8.03 (t, $H^{4,4''}$ tpy, J_{HH} = 8.0, 2H), 7.99 (d, $H^{a\ or\ b}$ py, J_{HH} = 4.8, 2H), 7.51 (dd, $H^{5,5''}$ tpy, J_{HH} = 7.8, 5.7 Hz, 2H) ppm. **L2** δ(CD_3OD, TMS). 8.78 (d, $H^{6,6''}$ tpy, J_{HH} = 3.7, 2H), 8.76 (s, $H^{3',5'}$ tpy, 2H), 8.69 (d, $H^{3,3''}$ tpy, J_{HH} = 7.9, 2H), 8.41 (s, H^{a} Im, 1H), 8.09 (d, $H^{2'''or3'''}$ Ph, J_{HH} = 8.6, 2H), 8.05 (td, $H^{4,4''}$ tpy, J_{HH} = 7.6 , 1.7, 2H), 7.89 (d, $H^{2'''or3'''}$ Ph, J_{HH} = 6.8, 2H), 7.88 (s, $H^{b\ or\ c}$ Im, 1H), 7.55 (dd, $H^{5,5''}$ tpy, J_{HH} = 6.4, 4.8, 2H), 7.17 (s, $H^{b\ or\ c}$ Im, 1H) ppm.

L3. It was obtained following the protocol described in the literature.[2] The NMR data are included as those reported were in a different solvent.^{1}H NMR: δ(CD_3OD, TMS). 8.77 (s, $H^{3',5'}$ tpy, 2H), 8.74-8.71 (m, $H^{3,3''}$, $H^{6,\ 6''}$ tpy, 4H), 8.25 (d, $H^{2'''or3'''}$ Ph, J_{HH} = 8.7, 2H), 8.20 (d, $H^{b\ or\ c}$ Im, J_{HH} = 2.0, 1H), 8.05 (td, $H^{4,4''}$ tpy , J_{HH} = 7.7, 1.8, 2H), 7.94 (d, $H^{2'''or3'''}$ Ph, J_{HH} = 8.7, 2H), 7.85 (d, $H^{b\ or\ c}$ Im, J_{HH} = 2.0, 1H), 7.53 (ddd, $H^{5,5''}$ tpy, J_{HH} = 5.5, 4.8, 1.2, 2H), 4.09 (s, MeIm, 3H) ppm.

---

[1] Wang, J, Hanan, G. S. A Facile Route to Sterically Hindered and Non-Hindered 4'-Aryl-2,2¢':6',2''-Terpyridines. *Synlett* **2005** (8) 1251-1254.

[2] Gupta S. K.; Choudhury, J. Templating an N-heterocyclic carbene (NHC)-cyclometalated Cp^*Ir^{III}-based oxidation precatalyst on a pendant coordination platform: assessment of the oxidative behavior via electrochemical, spectroscopic and catalytic probes. *Dalton Trans*., **2015**, 44, 1233-1239.

[3] Wang, C. X.; Li, L.; Yu, W. T.; Yang, J. X.; Wu, J. Y. 400-[4-(Imidazol-1-yl)phenyl]-2,2':6',2''-terpyridine (IPTP), Acta Cryst. 2006, E62, o246–o248.

General pattern of the ^{1}H NMR spectra.

The ligands are symmetric in all complexes. The resonances of $H^{6,6''}$ (doublet with a J_{HH} about 4 Hz) and $H^{3,3''}$ (doublet with a J_{HH} about 8 Hz) appear at higher field than the doublets of doublets or triplets of the $H^{4,4''}$ and $H^{5,5''}$ signals. For **L2** and **L3** complexes, the resonances of the phenyl group are observed as doublets with J_{HH} about 8-9 Hz in the region 7.9-8.6 ppm and the imidazolyl protons give rise to singlets or doublets with J_{HH} lower than 2Hz.

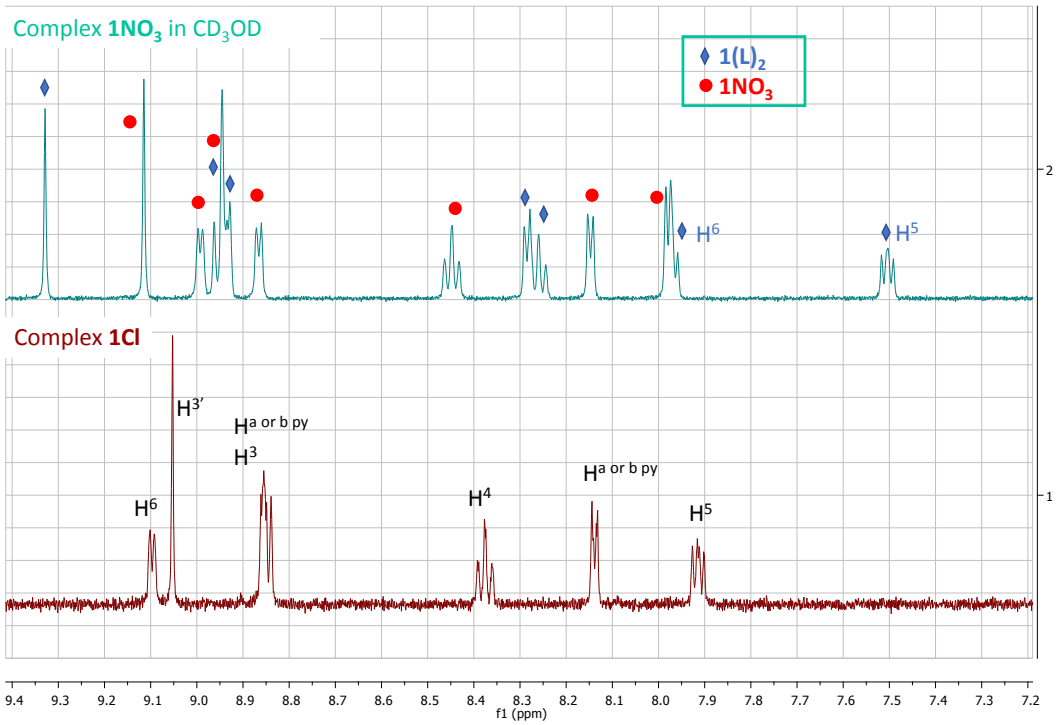

Fig. S1. ^{1}H NMR spectra of complexes **1Cl** and **$1NO_3$** in CD_3OD. Complex **$1NO_3$** evolves in solution to give a mixture of **$1NO_3$** and **$1(L)_2$**, in a 66:33 ratio.

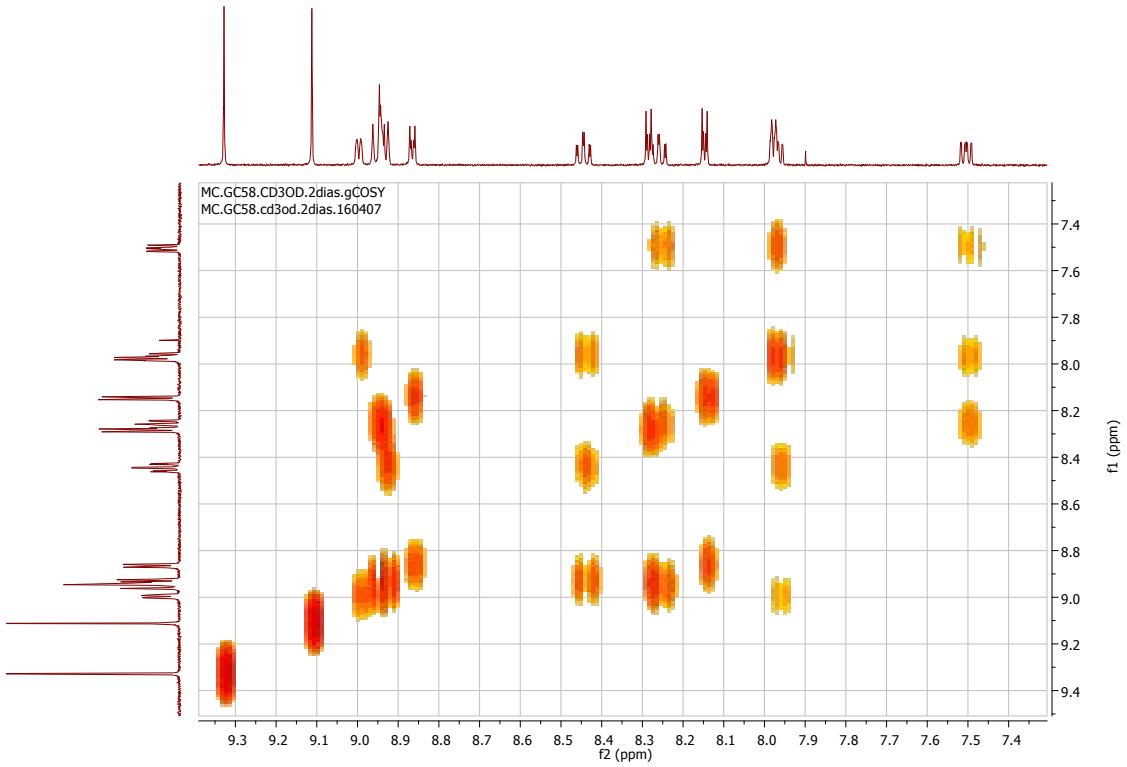

Fig. S2. COSY of the mixture of **1NO$_3$** and **1(L)$_2$** as the former is solved in CD_3OD

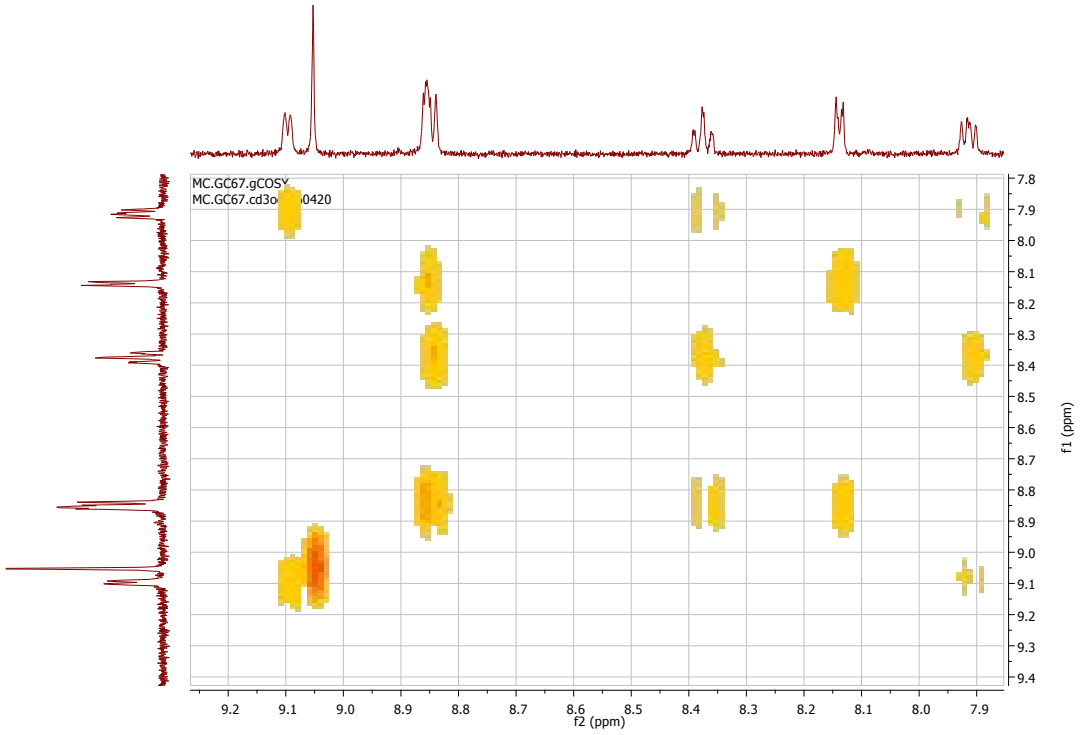

Fig. S3. COSY of **1Cl** in CD_3OD

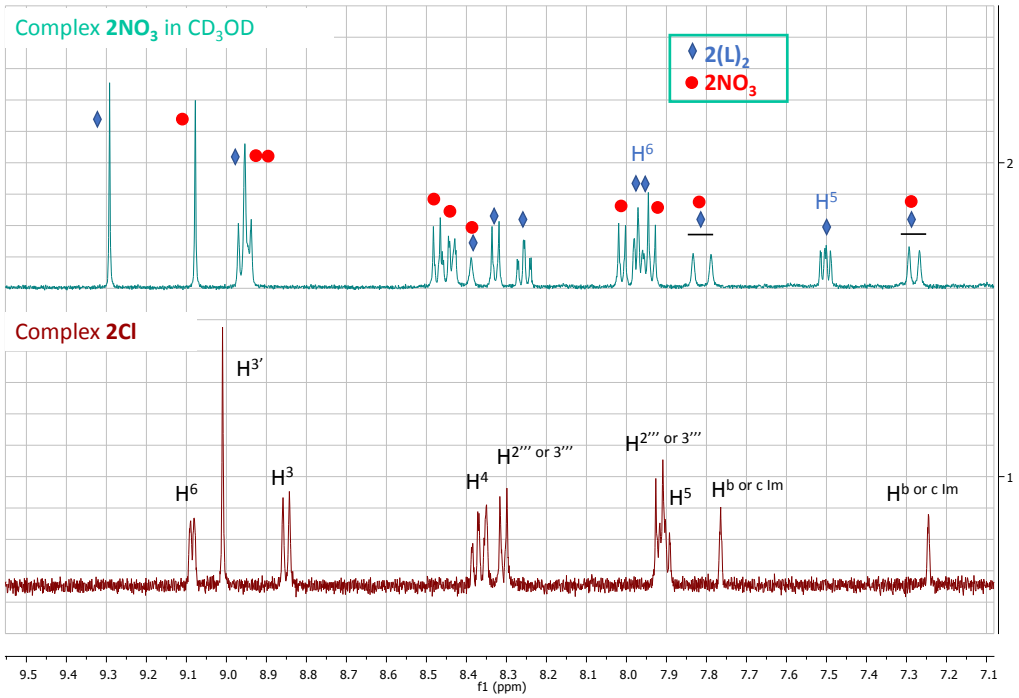

Fig. S4. ^{1}H NMR spectra of complexes **2Cl** and **2NO$_3$** in CD_3OD. Complex **2NO$_3$** evolves in solution to give a mixture of **2NO$_3$** and **2(L)$_2$**, in a 69:31 ratio.

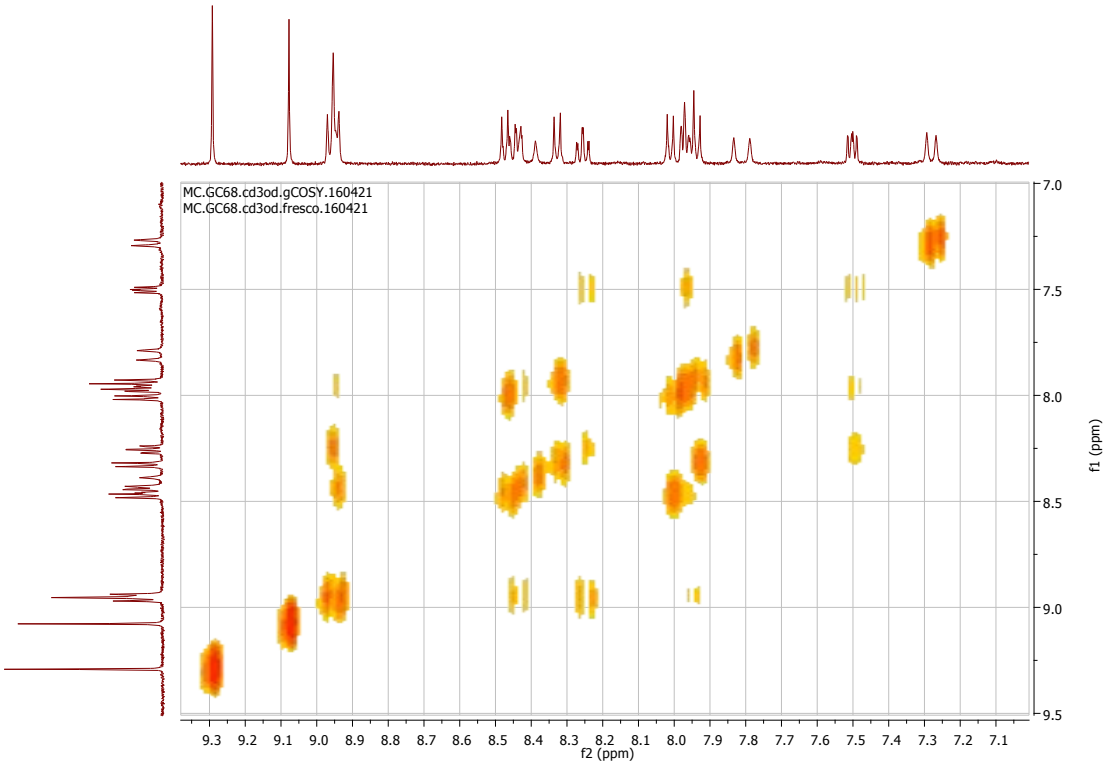

Fig. S5. COSY of the mixture of **2NO$_3$** and **2(L)$_2$** as the former is solved in CD_3OD

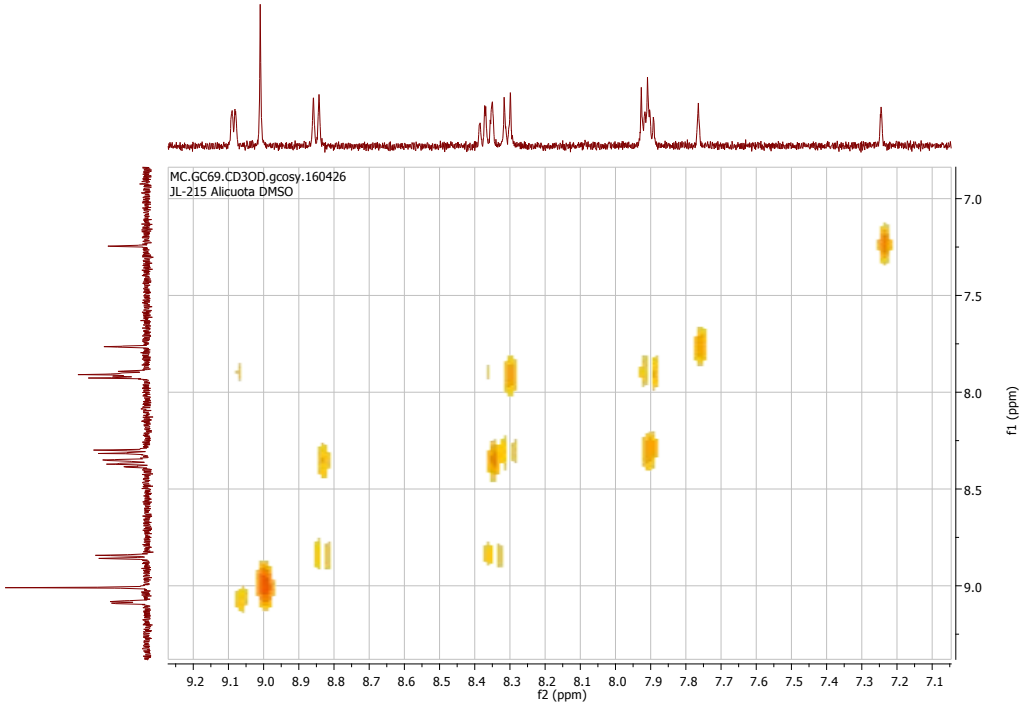

Fig. S6. COSY of **2Cl** in CD_3OD

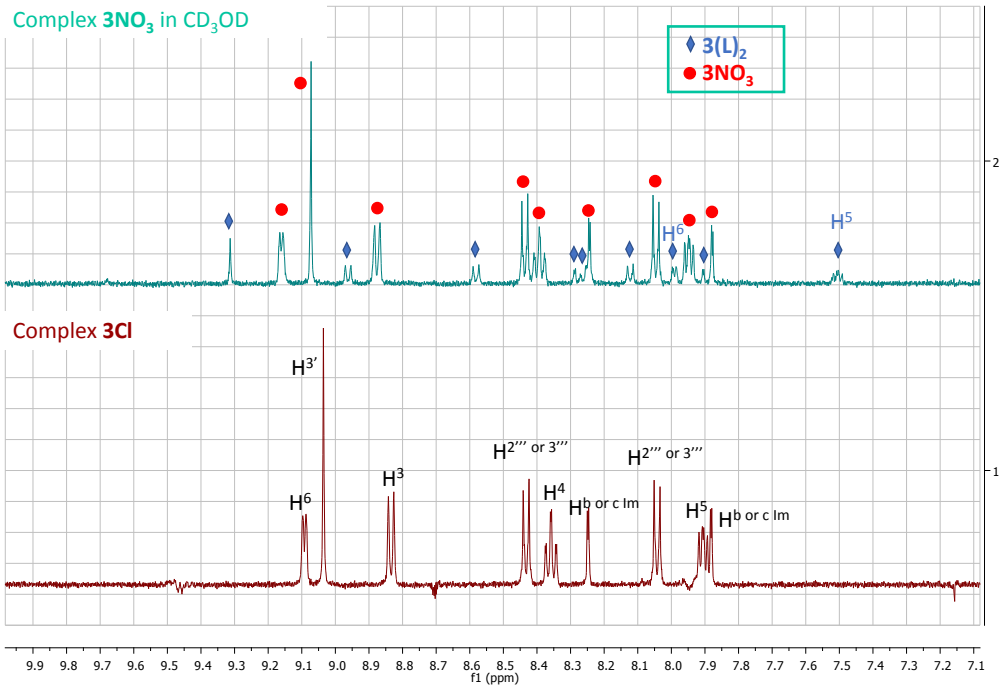

Fig. S7. ^{1}H NMR spectra of complexes **3Cl** and **$3NO_3$** in CD_3OD. Complex **$3NO_3$** evolves in solution a mixture of **$3NO_3$** and **$3(L)_2$**, in a 82:18 ratio.

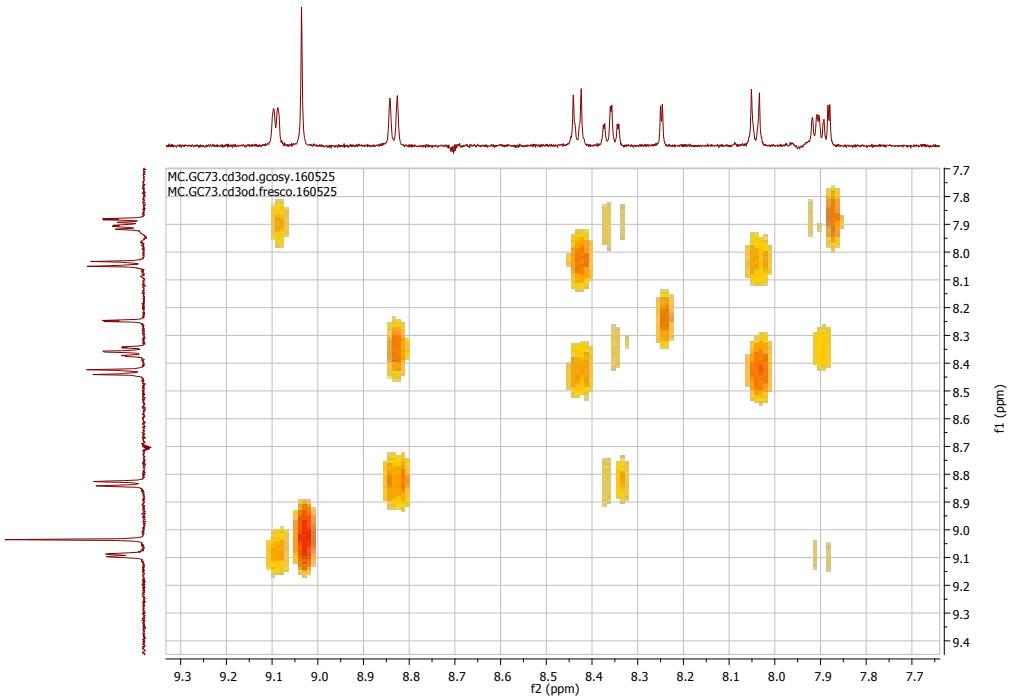

Fig. S8. COSY of **3Cl** in CD_3OD

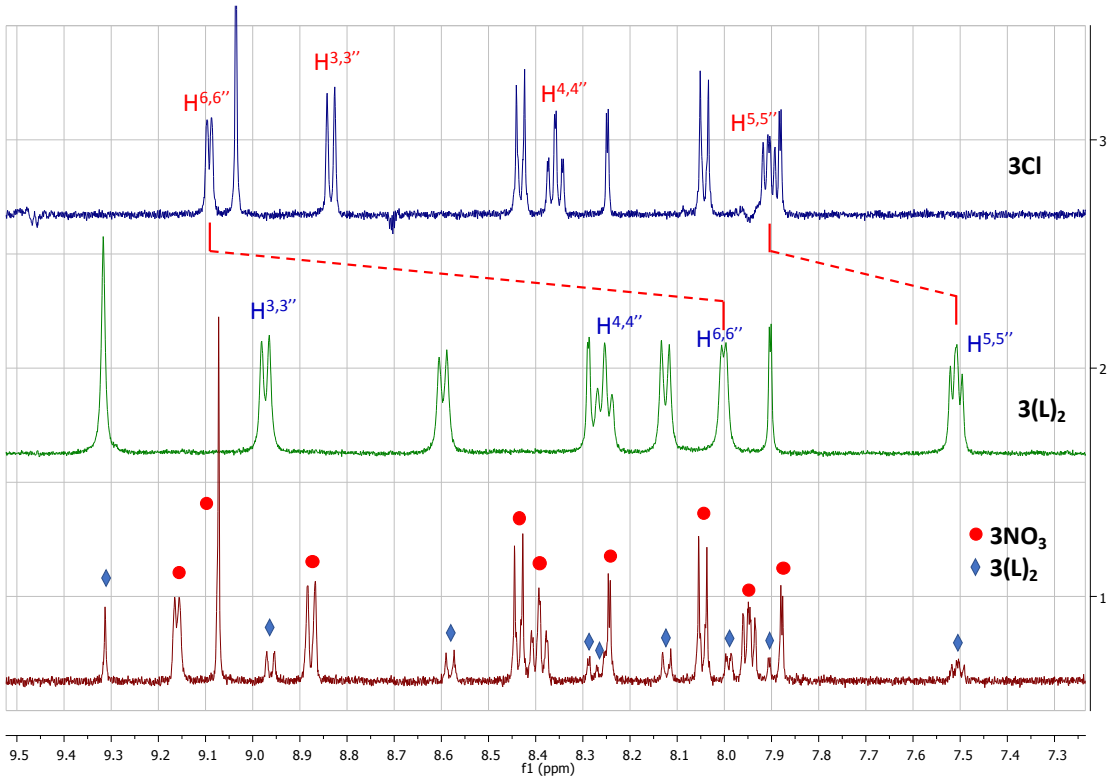

Fig. S9. ^1H NMR spectra (CD_3OD) for complexes **3Cl** (top), **3(L)$_2$** (middle) and the mixture obtained in the solution of $Zn(NO_3)_2 \cdot 6H_2O$ and **L3** in a 1:1 molar ratio in CD_3OD (down).

(a)

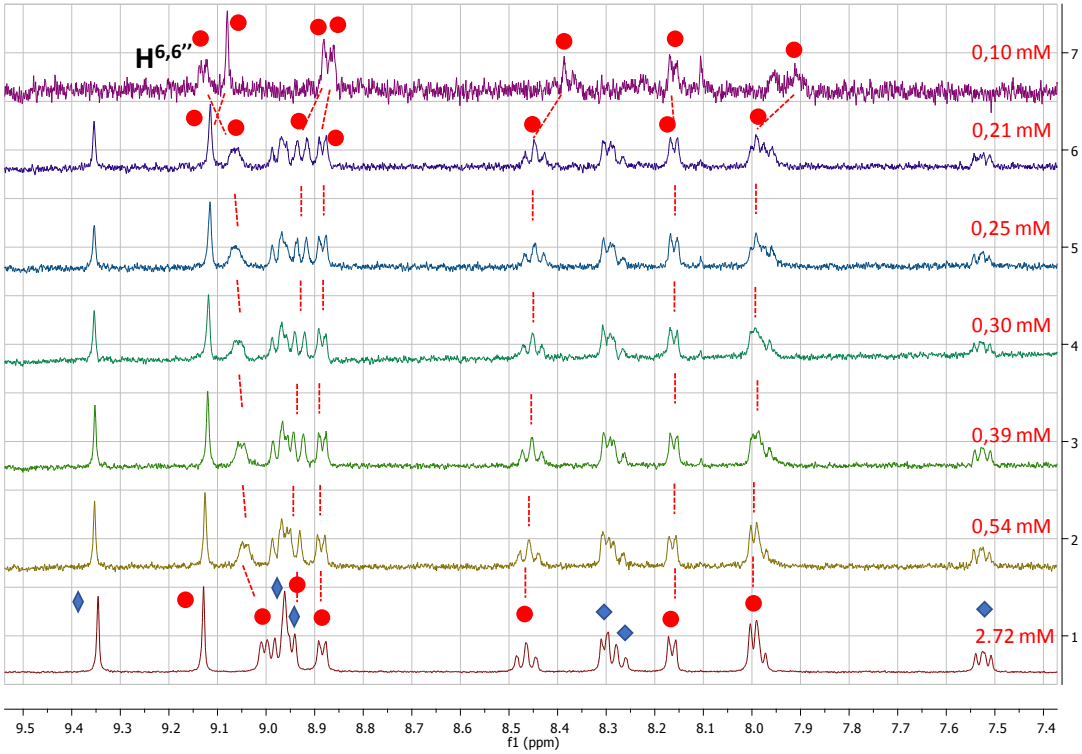

(b)

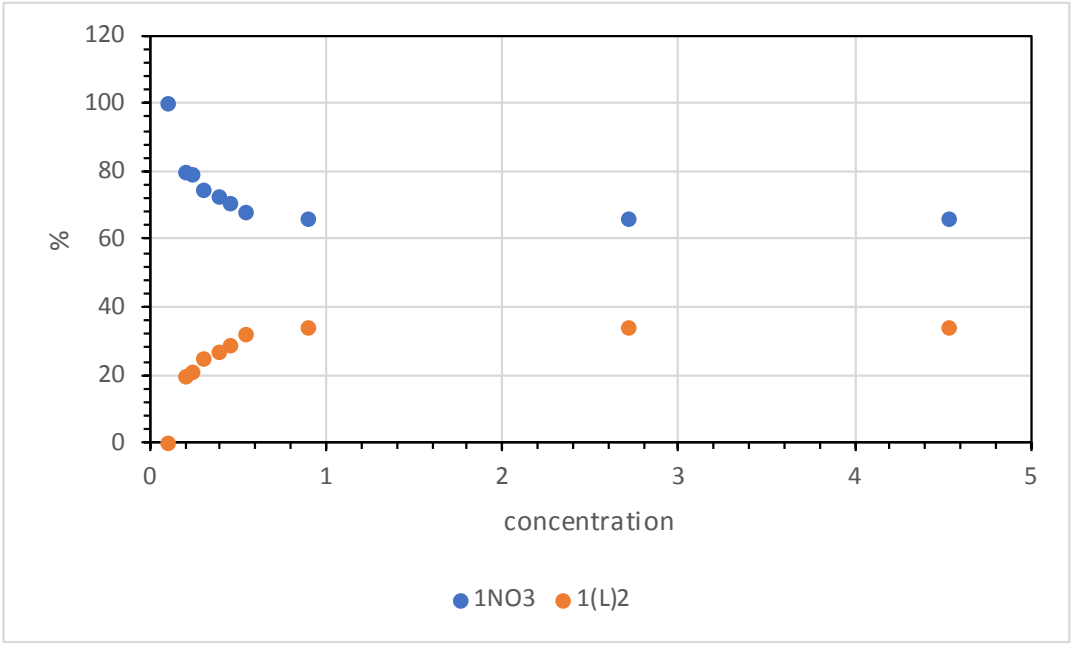

Fig. S10. a) ^{1}H NMR spectra obtained after dissolving **1NO$_3$** in CD_3COD solution, at different initial concentrations of **1NO$_3$** (mM). b) Representation of the percentage of the **1NO$_3$** and **1(L)$_2$** species against initial concentration of **1NO$_3$** (mM).

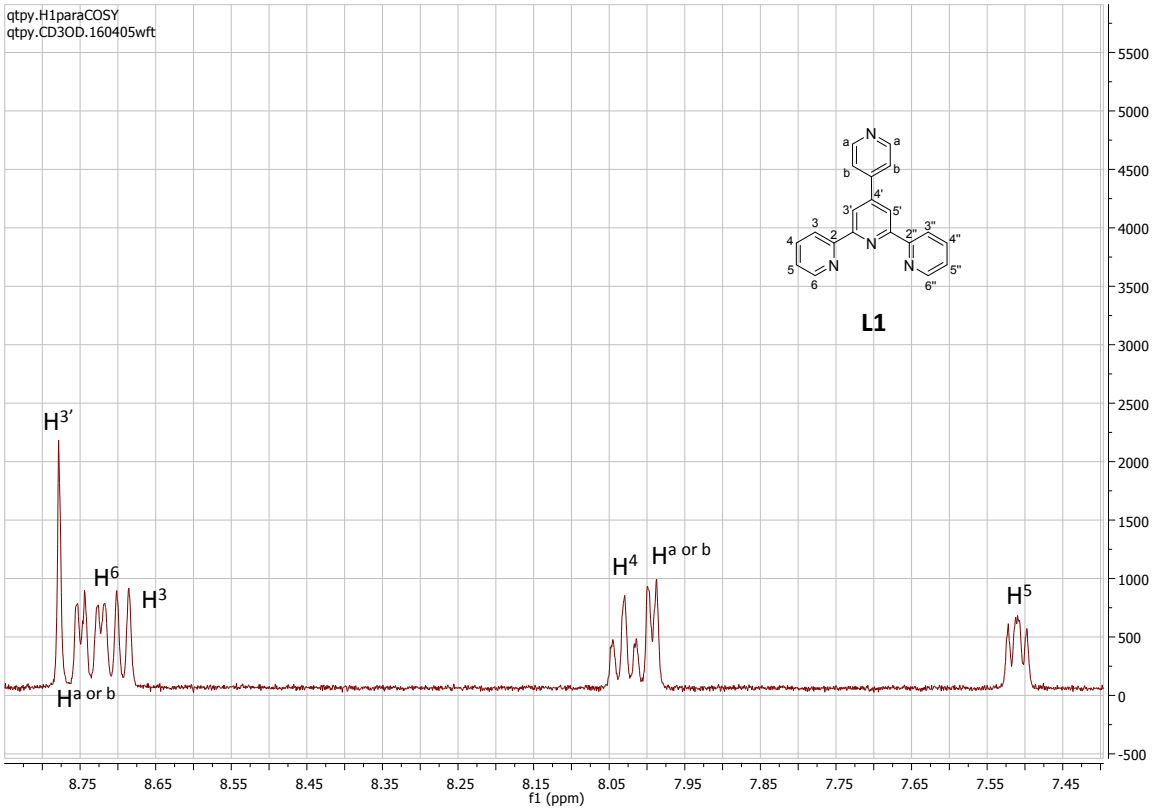

Fig. S11. ^{1}H NMR spectrum of ligand **L1** in CD_3OD.

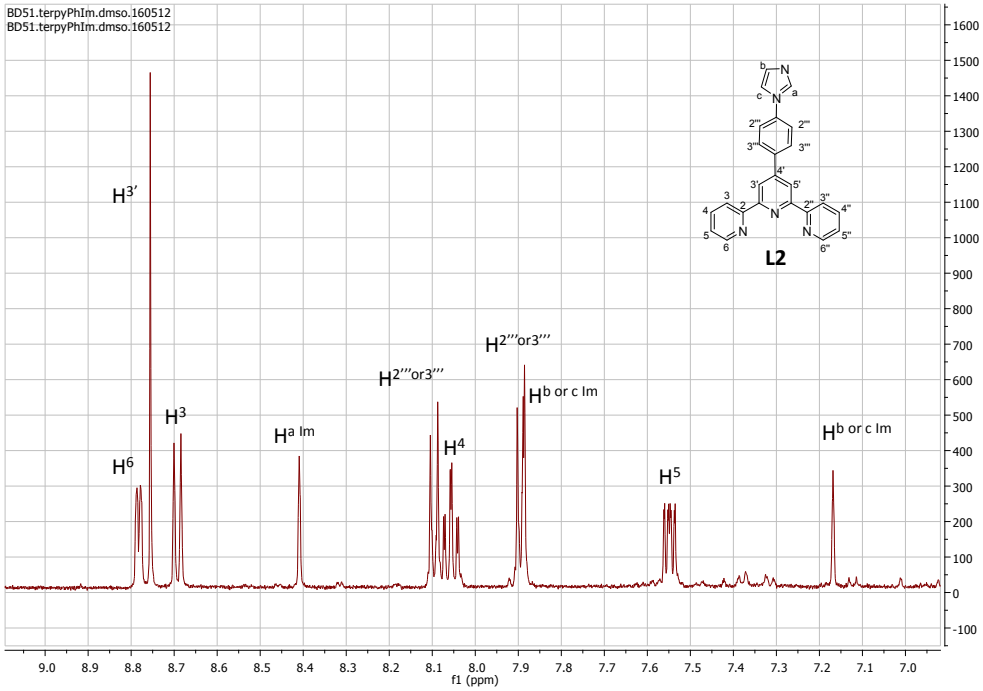

Fig. S12. ^{1}H NMR spectrum of ligand **L2** in DMSO-d_6.

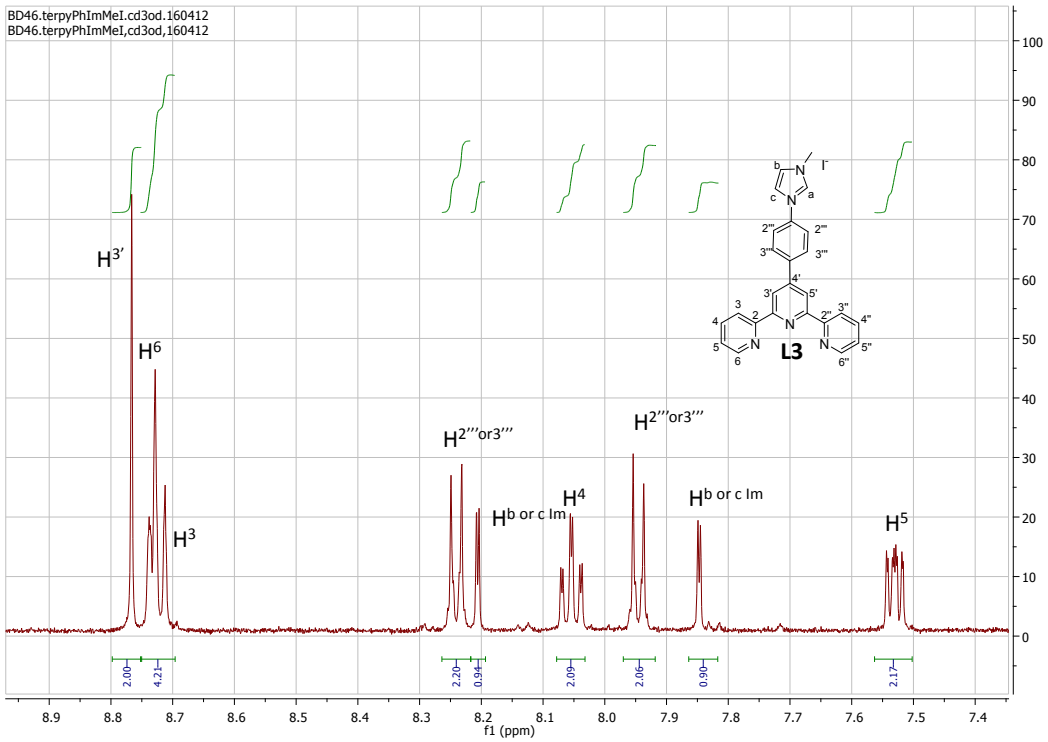

Fig. S13. ^{1}H NMR spectrum of ligand **L3** in CD_3OD.

FAB Mass Spectrometry

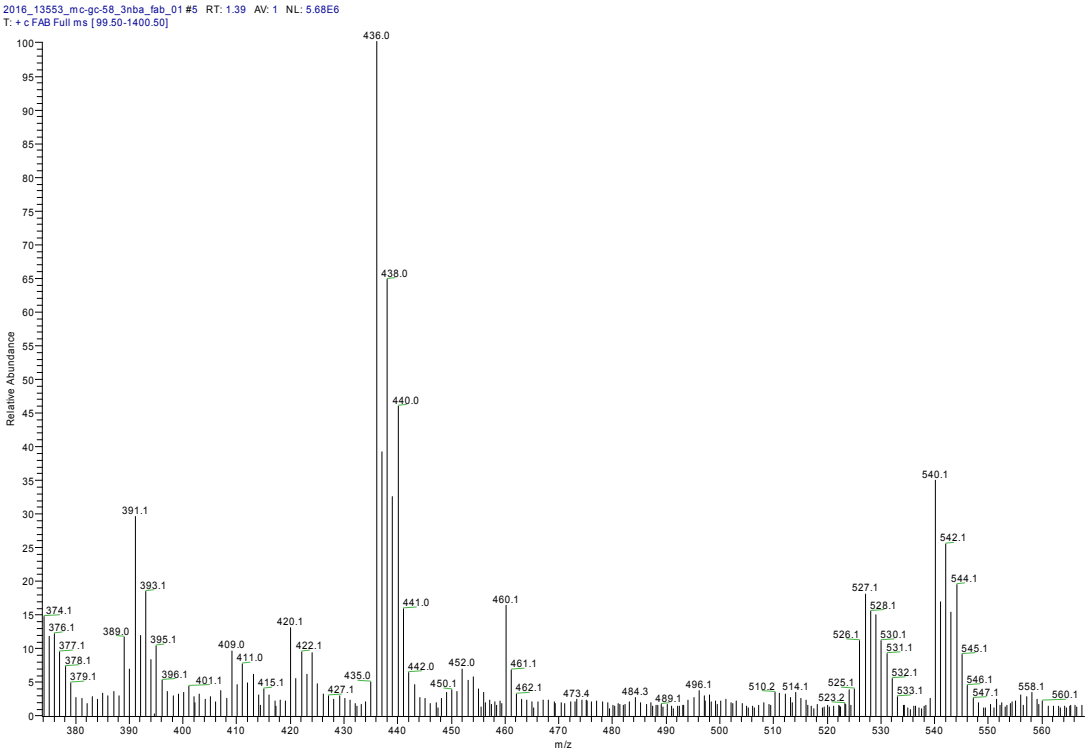

Fig. S14. FAB+ spectrum of **1NO$_3$**.

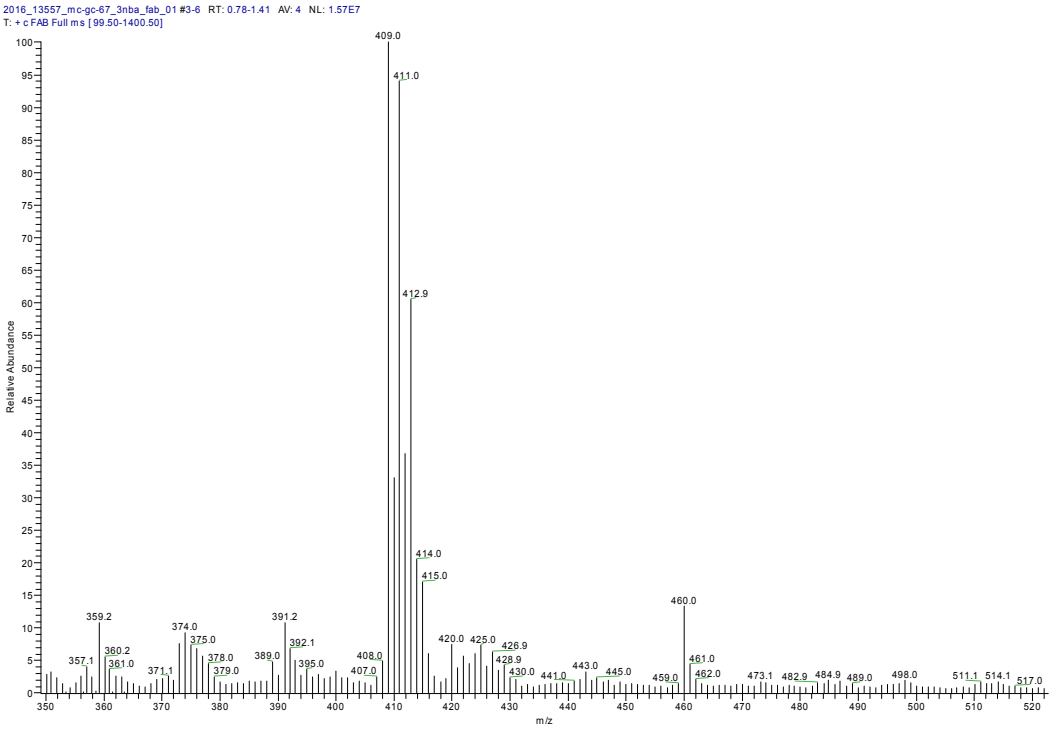

Fig. S15. FAB+ spectrum of **1Cl**.

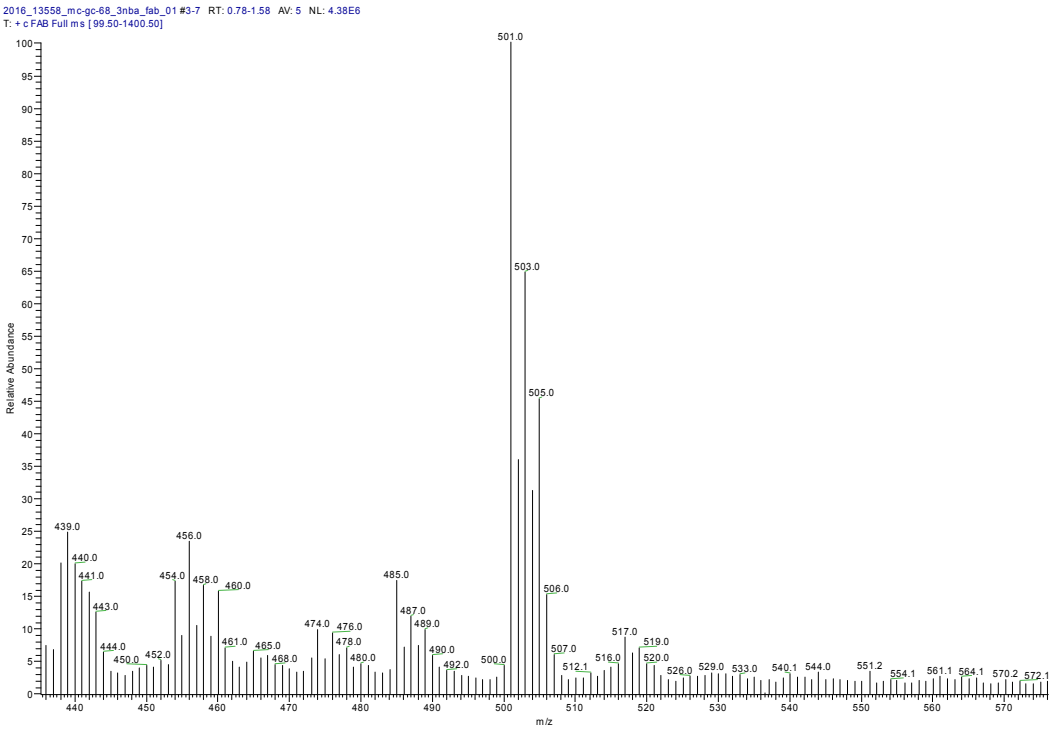

Fig. S16. FAB+ spectrum of complex **2NO$_3$**.

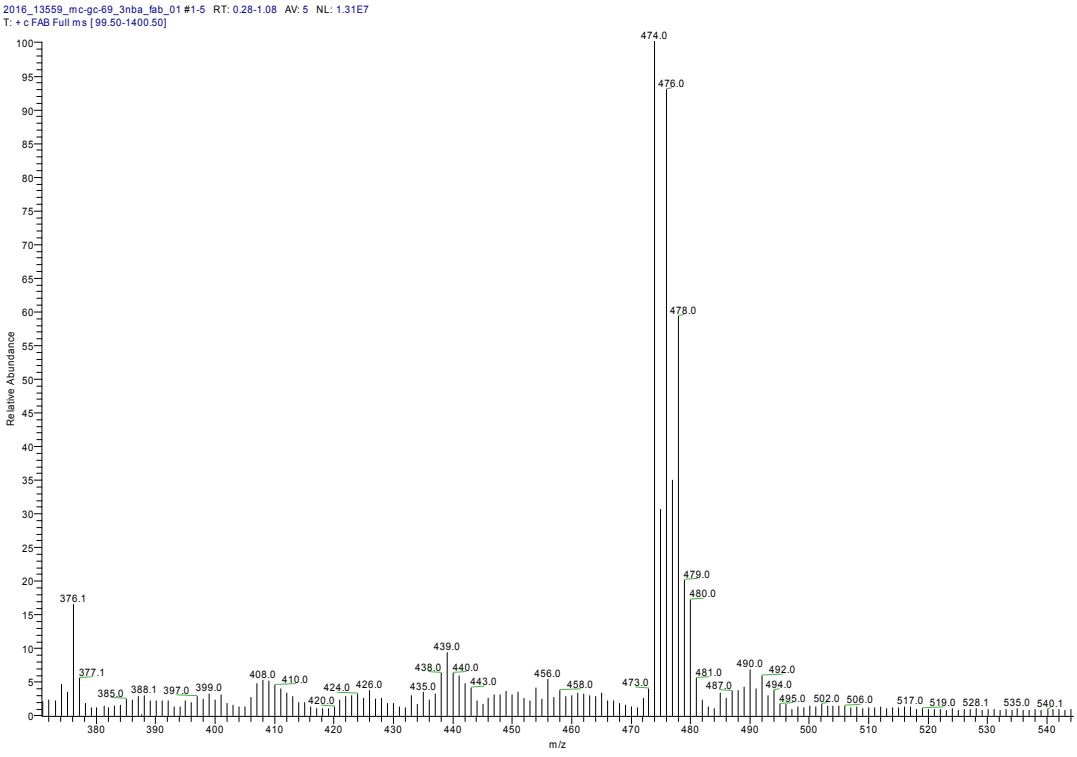

Fig. S17. FAB+ spectrum of **2Cl**.

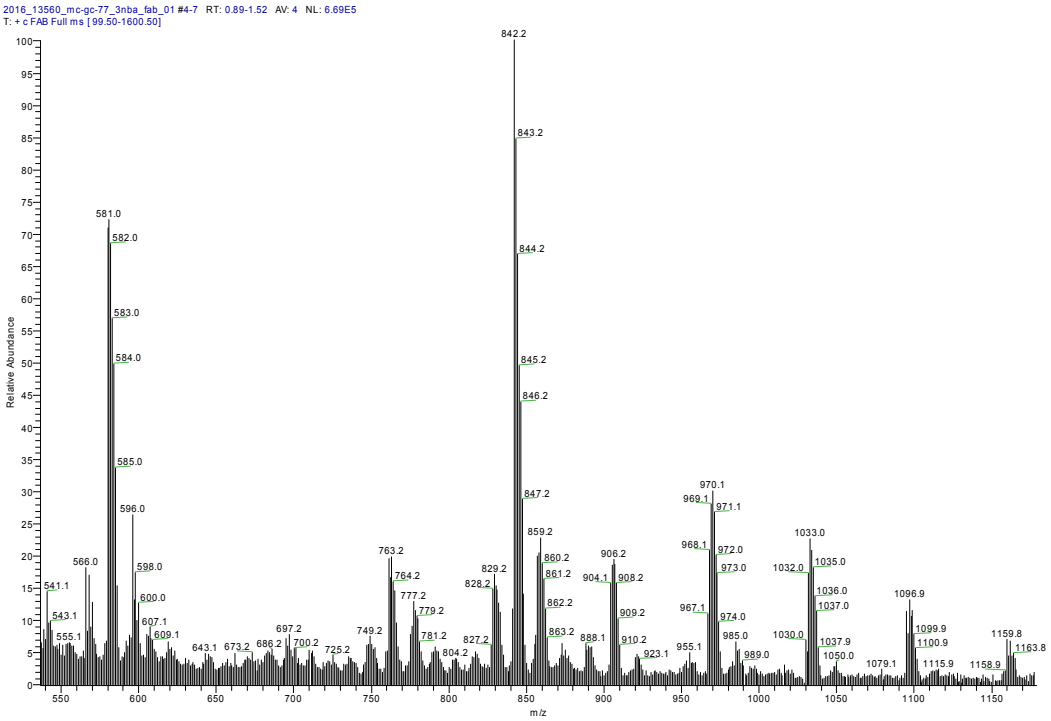

Fig. S18. Region of the FAB+ spectrum of **3(L)$_2$**.

Stability and aquation of 3Cl and $3(L)_2$

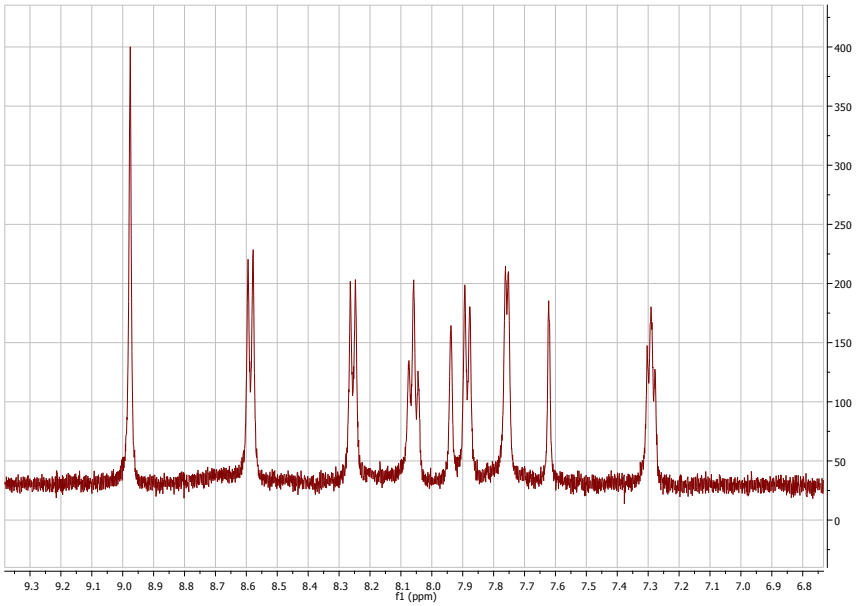

Fig. S19. ^{1}H NMR spectrum of **$3(L)_2$** in D_2O.

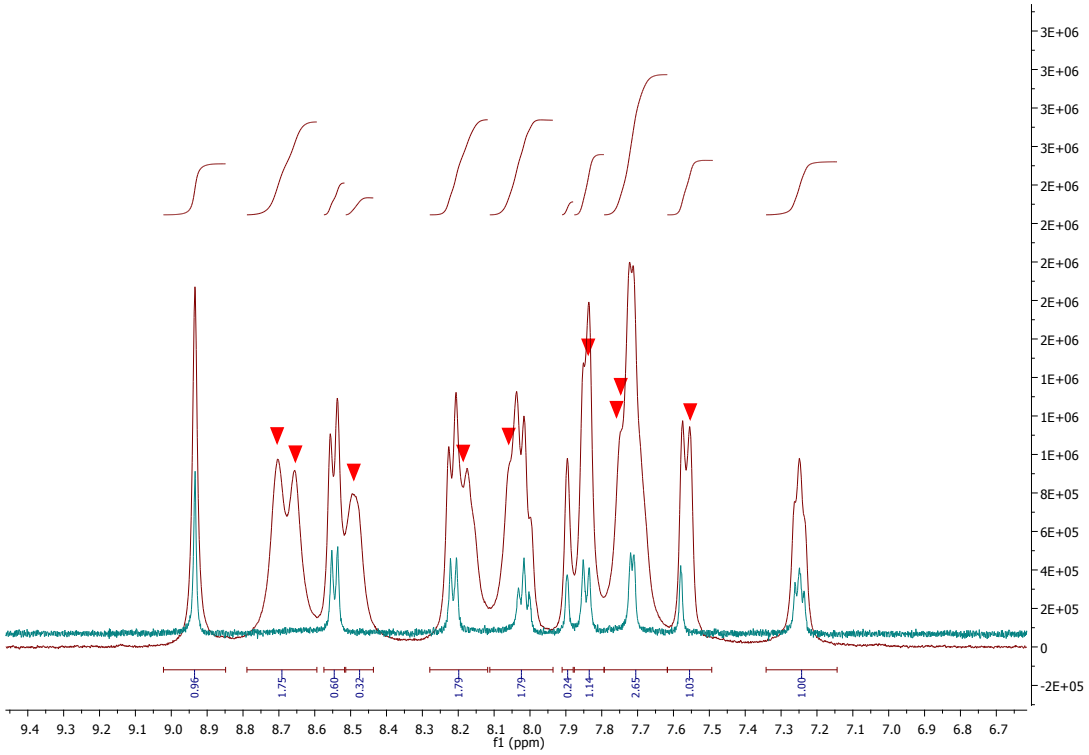

Fig. S20. ^{1}H NMR spectrum of **3Cl** in D_2O (4.7 mM) (brown color). It is included in green the ^{1}H NMR spectrum of 3(L)2. Red triangles indicate the position of resonances of the solvated forms of **3Cl**

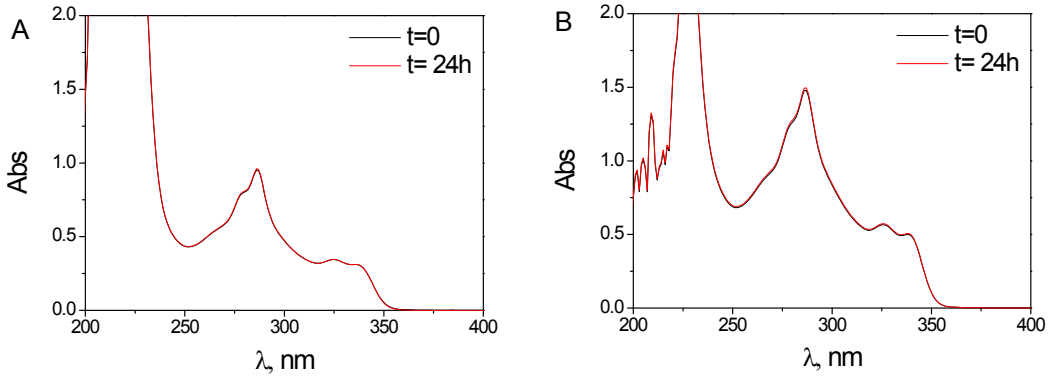

Fig. S21. Absorbance spectra of 21 µM **3Cl** (A) and 30 µM **3(L)$_2$** (B) of freshly prepared solutions (-) and after 24h (-). I = 0.1 M, pH = 7 and T = 25°C.

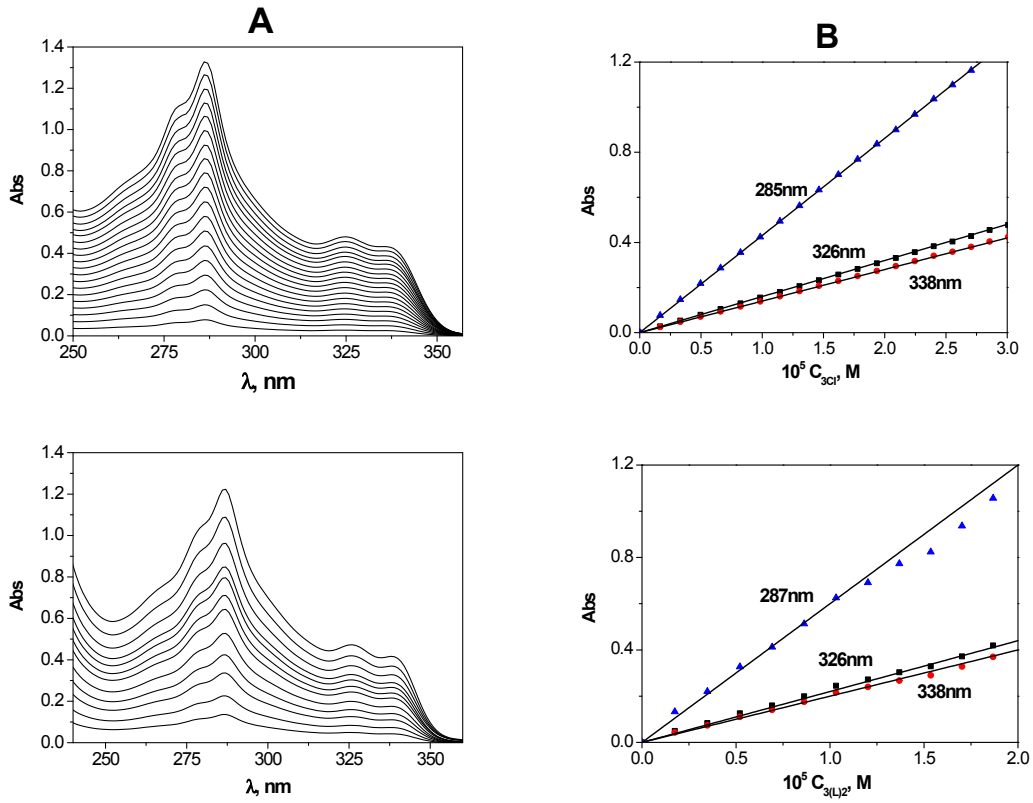

Fig. S22. A) Absorbance spectra of **3Cl** (top) and **3(L)$_2$** (bottom) at different dye concentrations; B) relevant absorbance/concentration plot at selected wavelengths. I = 0.1 M, pH = 7 and T = 25°C.

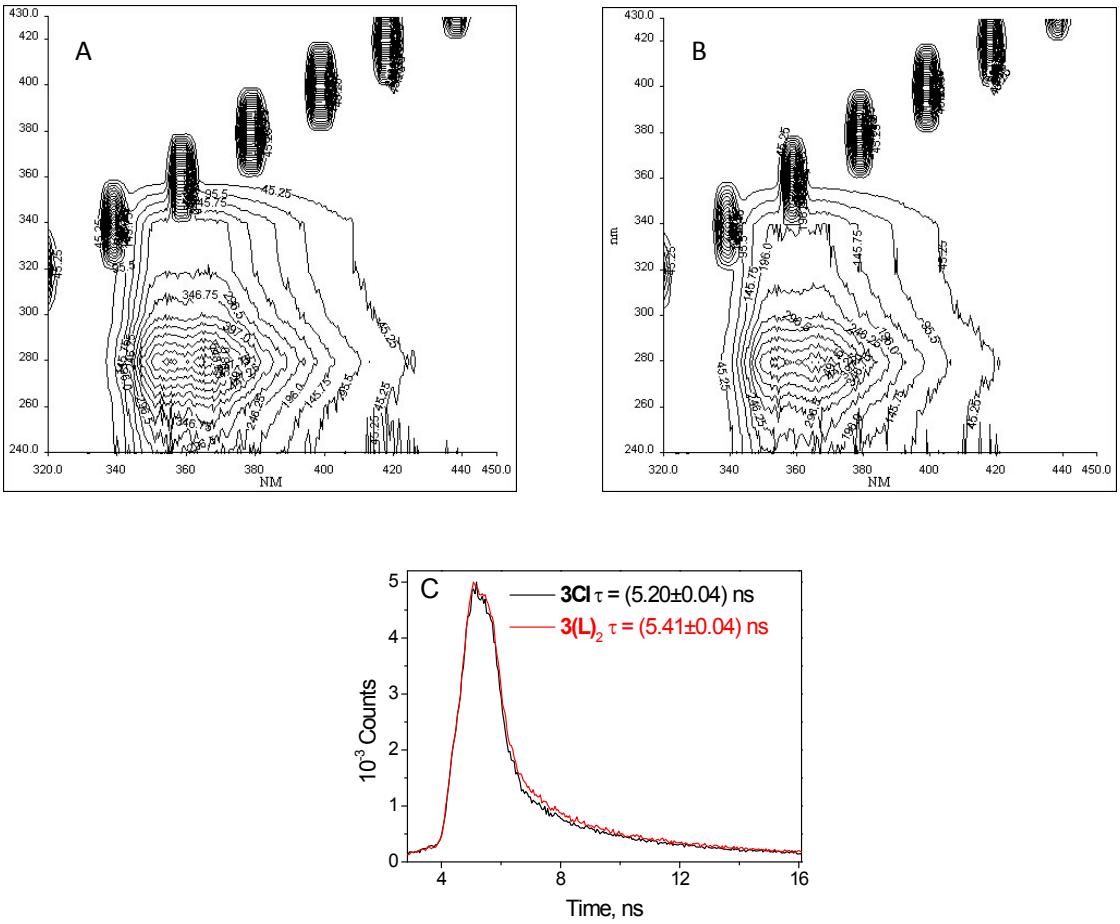

Fig. S23. A) Fluorescence 3D spectra of **3Cl** ($C_D = 6.5\times10^{-7}$ M) and B) **3(L)$_2$** ($C_D = 5.0\times10^{-6}$ M), x-axis, emission wavelength = 320 – 450 nm; y-axis, excitation wavelength = 240 – 430 nm). C) Time-correlated single photon counting decay of **3Cl** and **3(L)$_2$,** C_D = 1 µM, I = 0.1 M, pH = 7 and T = 25°C.

$3(L)_2$ – ctDNA interaction

Spectrophotometric titrations show that, upon duplex addition to a **$3(L)_2$** solution, two isosbestic points appear (at 320 and 343 nm), indicating the existence of several species in equilibria (Fig. S23A). No quantification of the binding constant was possible as quantitative binding was found to occur (Fig. S23B). Nevertheless, the equilibrium constant was calculated from the spectrofluorimetric titration in which a fluorescence decrease was observed upon duplex addition (Fig. S23C). The Schatchard model (eq. 1) was applied to the spectrofluorometric data, leading to the determination of both the binding constant, K_{SC} and the site size, *n*.

$$\frac{r}{[D]} = \frac{K_{SC}}{n} - K_{SC}r \qquad [1]$$

In this model, $r = [\text{D-DNA}]/C_{DNA} = \Delta F/(\Delta\delta C_{DNA})$, D is the free zinc complex, D-DNA is the dye/DNA adduct, C_{DNA} is the total analytical concentration of the polynucleotide and $\Delta\delta = \delta_{D\text{-}DNA} - \delta_D$ is the amplitude of the binding isotherm (Fig. S23D). The Scatchard analysis (Fig. S23E) reveals that **$3(L)_2$** interacts with DNA double helix with a $K_{SC} = (2.3 \pm 0.3) \times 10^5\ M^{-1}$ and $n = 2.3$.

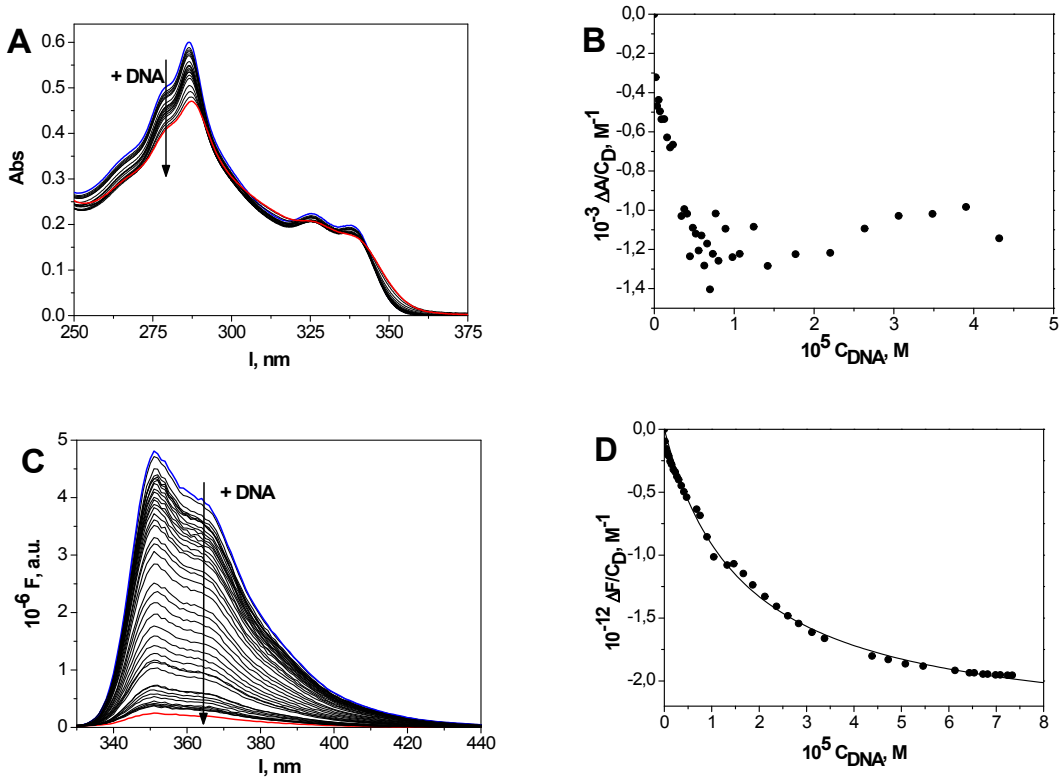

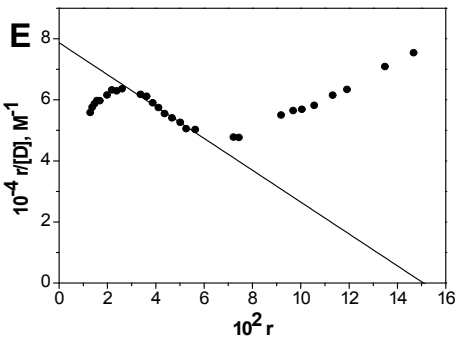

Fig. S24. Spectrophotometric titrations for the **3(L)$_2$**/DNA system (A) and relevant binding isotherm at 287 nm (B); $C_D = 1.0\times10^{-5}$ M, C_{DNA} from 0 to 4.7×10^{-5} M. Spectrofluorometric titration for the **3(L)$_2$** /DNA system, (C) relevant binding isotherm at λ_{exc} = 287 nm, λ_{em} = 351 nm (D) and Scatchard plot (E); $C_D = 2.2\times10^{-6}$ M, C_{DNA} = 0 to 7.6×10^{-5} M. I = 0.1 M, pH = 7 and T = 25°C.

Circular dichroism (CD) experiments where increasing amounts of **3(L)$_2$** were added to a ctDNA solution show the appearance of an isodichroic point at 327 nm, a bathochromic shift of the DNA positive band and an induced negative band at 343 nm that would agree with partial intercalation of **3(L)$_2$** into duplex DNA (Fig. S24A). By contrast, viscosimetric experiments (Fig. S24B) do not show the helix elongation that would had been occurred for Zn complex intercalation. Indeed, some DNA compaction can be observed under these more concentrated conditions. Viscosimetric experiments were done by recording the time flow through an Ubbelhode capillary (5 repeats to be averaged) of the sample at different C_D/C_{DNA} ratios ($t_{D\text{-}DNA}$), of DNA alone (t_{DNA}) and of the buffer alone (t_{solv}). The relative viscosity, η/η_0, is then calculated according to eq. 2.

$$\eta/\eta_0 = (t_{D\text{-}DNA} - t_{solv})/(t_{DNA} - t_{solv}) \qquad [2]$$

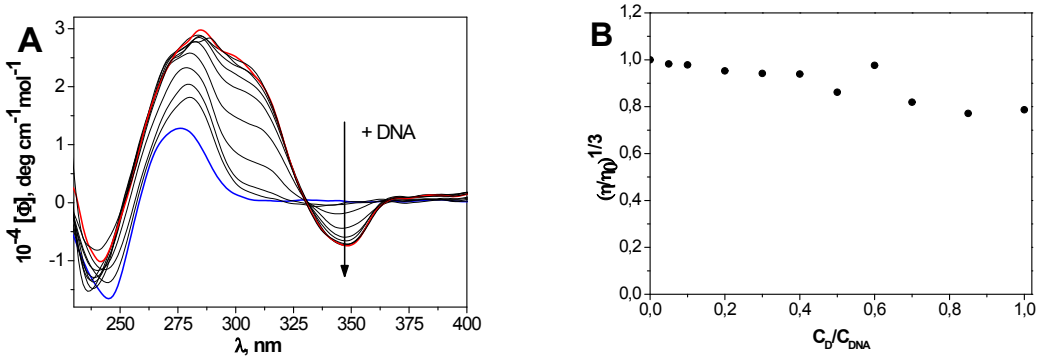

Fig. S25. CD titration for the **3(L)$_2$** /DNA system (A); $C_{DNA} = 3.9\times10^{-5}$M, C_D from 0 to 7.8×10^{-5} M. Viscosimetric titration (B); $C_{DNA} = 2.0\times10^{-4}$ M, C_D from 0 to 1.6×10^{-4} M. I = 0.1M, pH = 7 and T = 25°C.

The binding has also been studied by a kinetic approach. The kinetic stopped-flow traces are single exponential (Fig. S25A). Their fitting enables time constant evaluation which depends on reactants concentration as shown in Fig. S25B.

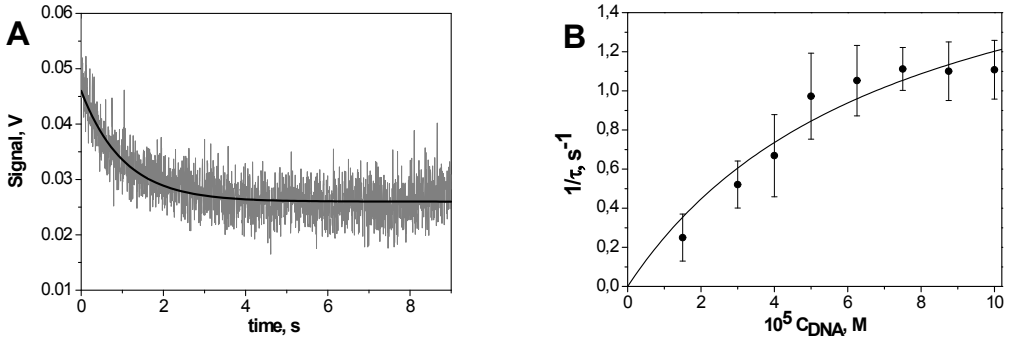

Fig. S26. Stopped-flow kinetic trace for **3(L)$_2$**/DNA system (A) and reciprocal time constant, 1/τ, dependence on reactants concentration. $C_D = 5.0\times10^{-5}$M, λ = 290 nm. I = 0.1 M, pH = 7 and T = 25°C.

The curvature observed suggests the existence of a pre-equilibrium, according to the mechanism below.

DNA + D ⇌ D-DNA* · D-DNA [3]

In [3] a very fast pre-equilibrium leads to the formation of the D-DNA* intermediate (with K_0 formation equilibrium constant), that in time evolves to the final D-DNA species. The zero intercept of the trend of Fig. S25B indicates that the second step is quantitative. On the basis of he above reaction scheme, data were fitted according to eq. 4.

$$\frac{1}{\tau} = \frac{K_0\, k_1 C_{DNA}}{1 + K_0 C_{DNA}} \qquad [4]$$

In agreement with the high charge borne by **3(L)$_2$**, K_0 is much higher ($K_0 = (1.4 \pm 0.5) \times 10^4$ M^{-1}, $k_1 = 2.1 \pm 0.4$ s^{-1}) than the value of 100 M^{-1} taken as the reference for purely electrostatic binding to DNA of a +1 charged dye at 0.1 M ionic strength.[4] Therefore, D-DNA* already accounts also for groove interaction and/or π–π interaction. Subsequent formation of D-DNA is related to quantitative formation of a more stable complex.

On the whole, it can be concluded that **3(L)$_2$** binds to the DNA duplex in a complex manner which is a combination of partial intercalation and groove binding. Total intercalation is excluded and the

[4] Biver, T.; Cavazza, C.; Secco, F.; Venturini, M. The Two Modes of Binding of Ru(Phen)2dppz2+ to DNA: Thermodynamic Evidence and Kinetic Studies. J. Inorg. Biochem. 2007, 101 (3), 461–469. https://doi.org/10.1016/j.jinorgbio.2006.11.009.

affinity for DNA is lower than that for the DNA G-quadruplex as it will be shown in the main manuscript.

Interaction of 3Cl and 3(L)$_2$ with Tel22

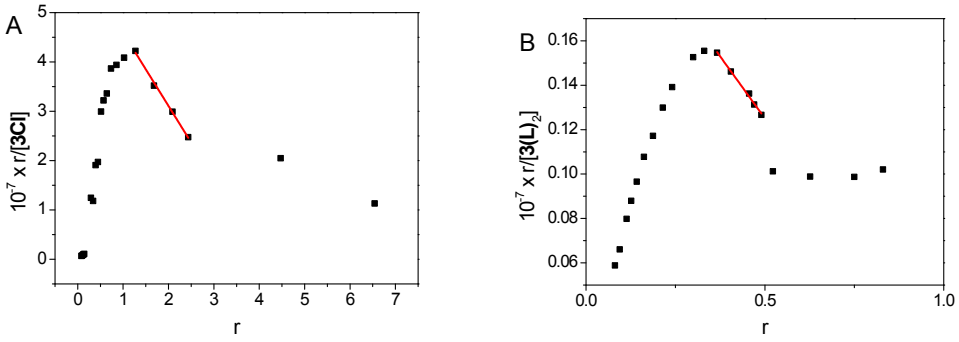

Fig. S27. Scatchard Plots of the fluorescence titrations of **3Cl** (A) and **3(L)$_2$** (B) with Tel22.

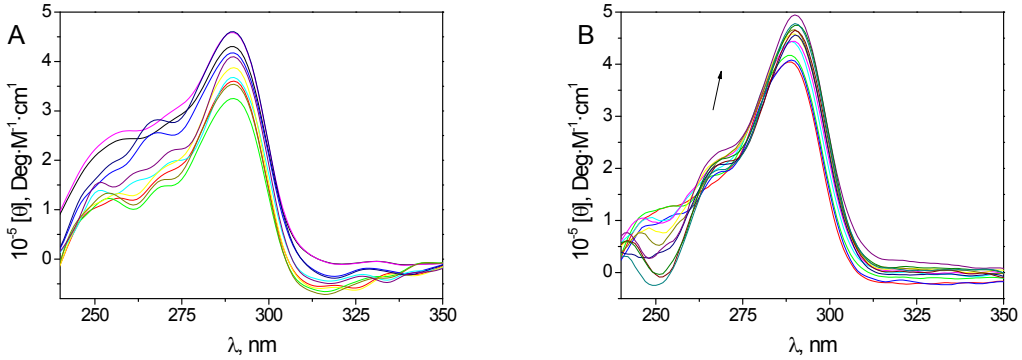

Fig. S28. CD spectra of Tel22 in the presence of different concentrations of **3Cl** (A) and **3(L)$_2$** (B). C_{Tel22} = 3.1 μM, I = 0.1 M, pH = 7 and T = 25 °C.